Using Google Earth Engine open-source code for land surface temperature estimation from Landsat data in Chuong My district, Hanoi city, Vietnam

Nguyen Thu Thuy[1], Vu Van Thai[2], Nguyen Khac Manh[1], Vu Van Truong[1], Ha Tri Son[1], Nguyen Thi Hai Van[3], Nguyen Hai Hoa[1*]

[1]*Vietnam National University of Forestry*

[2]*Green Field Consulting & Development Ltd.*

[3]*Hanoi University*

Sử dụng mã nguồn mở Google Earth Engine để ước tính nhiệt độ bề mặt đất từ dữ liệu ảnh Landsat tại huyện Chương Mỹ, thành phố Hà Nội, Việt Nam

Nguyễn Thu Thủy[1], Vũ Văn Thái[2], Nguyễn Khắc Mạnh[1], Vũ Văn Trường[1], Hà Trí Sơn[1], Nguyễn Thị Hải Vân[3], Nguyễn Hải Hòa[1*]

[1]*Trường Đại học Lâm nghiệp*

[2]*Công ty TNHH Tư vấn và Phát triển Đồng Xanh*

[3]*Trường Đại học Hà Nội*

**Corresponding author: hoanh@vnuf.edu.vn*

https://doi.org/10.55250/jo.vnuf.9.2.2024.097-106

Article info:
Received: 24/05/2024
Revised: 26/06/2024
Accepted: 29/07/2024

Keywords:
Emissivity, Land surface temperature, Landsat, NDVI.

ABSTRACT

Land surface temperature (LST) in association with urbanization has significantly influenced on local climates and terrestrial surface processes. By using multi-temporal Landsat data in the GEE platform, the study has found that there have been changes in land covers due to the main drivers of industrial development, urban and built-up expansion. This study estimated land surface temperature (LST) in Chuong My district from Landsat 5, 7, 8 and 9 thermal infrared sensors, using different surface emissivity sources. The Google Earth Engine (GEE), an advanced earth science data and analysis platform, offers the estimation of LST products, covering the time period from 2000 to 2024 in study site. RF algorithm for land cover classification and mapping is suggested to be applied in Chuong My district, with overall accuracy of land cover mapping in 2024 being 91.9% with Kappa coefficient of 0.89. The period 2000-2010 showed that 327.0 ha of land were converted to land for industrial development, urban and residential land, while the period 2010-2024 continued to witness a continued conversion of land to other land use purposes, with a decrease in agricultural land area (65.7 ha) and an increase in industrial land use (65.2 ha), but the rate of conversion was much lower than the previous period (2000-2024). The periods of 2000-2010 and 2010-2024 showed that there have been significant changes in land surface temperature. Most of the surface temperature in the entire region increased by over 2^0C, especially in the period 2003-2015 when a total area of 1424 ha had the temperature increased by above 3^0C. This is a consequence of the process of urbanization and industrialization, which began to take place in 2008, along with the process of changing the land cover status of the study area. Further studies are needed to better understand the thermal conductivity of surface materials and to plan how to reduce LST in such areas.

Từ khóa:
Độ phát xạ, Landsat, NDVI, nhiệt độ bề mặt đất.

TÓM TẮT

Nhiệt độ bề mặt đất kết hợp với quá trình đô thị hóa đã ảnh hưởng đáng kể đến khí hậu địa phương và các quá trình bề mặt đất. Bằng cách sử dụng dữ liệu Landsat đa thời gian trong nền tảng GEE, nghiên cứu đã phát hiện ra rằng đã có những thay đổi về độ che phủ đất do các động lực chính của phát triển công nghiệp, mở rộng đô thị và xây dựng. Thuật toán phân loại rừng ngẫu nhiên (RF) được sử dụng để phân loại lớp phủ mặt đất cho kết quả độ chính xác tổng thể là 91,9% với chỉ số Kappa là 0,89, thuật toán RF được đề xuất áp dụng tại khu vực nghiên cứu. Giai đoạn 2000-2010

có 327,0 ha đất được chuyển đổi sang đất phát triển công nghiệp, đất đô thị và đất ở, trong khi giai đoạn 2010-2024 tiếp tục chứng kiến tình trạng chuyển đổi đất sang mục đích sử dụng khác tiếp tục, tỷ lệ đất nông nghiệp giảm. Diện tích đất (65,7 ha) và tăng sử dụng đất công nghiệp (65,2 ha), nhưng tỷ lệ chuyển đổi thấp hơn nhiều so với giai đoạn trước (2000-2024). Giai đoạn 2000-2010 và 2010-2024 cho thấy nhiệt độ bề mặt đất liền có sự biến đổi rõ rệt, phần lớn nhiệt độ bề mặt toàn vùng tăng trên 2^0C, đặc biệt là giai đoạn 2003-2015 với tổng diện tích là 1.424 ha. nơi nhiệt độ tăng lên trên 3^0C. Đây là hệ quả của quá trình đô thị hóa, công nghiệp hóa bắt đầu diễn ra từ năm 2008 và quá trình thay đổi hiện trạng thảm phủ khu vực nghiên cứu.

1. INTRODUCTION

Land surface temperature (LST) is an important parameter for environmental studies, which uses the monitoring of landscape processes and responses [1], including the early detection of forest fires, risks of drought, water balance [2-3]. To better understand the progress of climate change which is often based on elements such as surface temperature, there is a need for frequent data provision to obtain the LST time series.

The Landsat 5, 7, 8 and 9 satellites carry thermal infrared radiometers, thus proved to be suitable for LST estimation. Over the last decades, there has been an increasing demand for satellite-derived surface temperature products [4]. Landsat-derived LST is largely used for urban temperature studies, especially for the study of the urban heat island phenomenon [5-7]. Many studies have used different algorithms and approaches for LST retrieval from Landsat [8-9]. Some of these algorithms have been employed in software tools, such as a plugin for the open-source software QGIS, to calculate LST from Landsat 5, 7, 8 imageries [10]. Similar tools have evolved for ERDAS software for processing Landsat 8 acquisition [11]. However, such tools require software installation and raw satellite data downloads which are extremely time-consuming.

The purpose of this study is to describe a method implemented in GEE platform that has been developed to provide fast and easy access to LST from the Landsat data. The approach uses a single channel (SC) algorithms to analyse Landsat 5, 7, 8, 9 thermal infrared observations. In the era of advanced information technology, the growing demand for LST data opens the path for new way for big data information exploration through the GEE. Using the online GEE platform offers the access to large catalogues of satellite imagery and planetary scale analysis capabilities. The LST estimation process is performed in the background on the Google cloud computing servers, with direct access to the GEE satellite data catalogue. Thus, the application only takes a relative short amount of time, which can be measured in seconds, to produce Landsat LST with no need for any computational resources from the user [4].

The objective of this study was to investigate the remote sensing thermal values in GEE platform to study the causes of the surface urban heat island (SUHI) effect of urbanization and industrialization. Specific objectives were formulated: (1) to construct the land use and land cover (LULC) and detect the changes in LULC; (2) to estimate the LST variability in Chuong My District; (3) to identify the autocorrelation between LST and changes in LULC; then discuss the negative impacts of the heat island.

2. RESEARCH METHODS

2.1. Study site

This study was conducted in Chuong My district, Hanoi city, which is located in 20.924 N and 105.704 E (Fig. 1). Chuong My is a district

of Hanoi in the Red Delta region of Vietnam, which is bordered by Ha Dong country; Thanh Oai to the East; Hoa Binh to the West; My Duc and Ung Hoa districts to the South; and Quoc Oai district to the North [13]. Chuong My is subdivided into 32 townships and communes. This district is well-known for its abundance of surface water resources, including a network of rivers and streams, which play a very important role in regulation of farming irrigation system and hydrologic cycles [13, 14]. However, agricultural and urban land use conversion have been the main drivers for water crisis, droughts, urban heat island, particularly in the summer season.

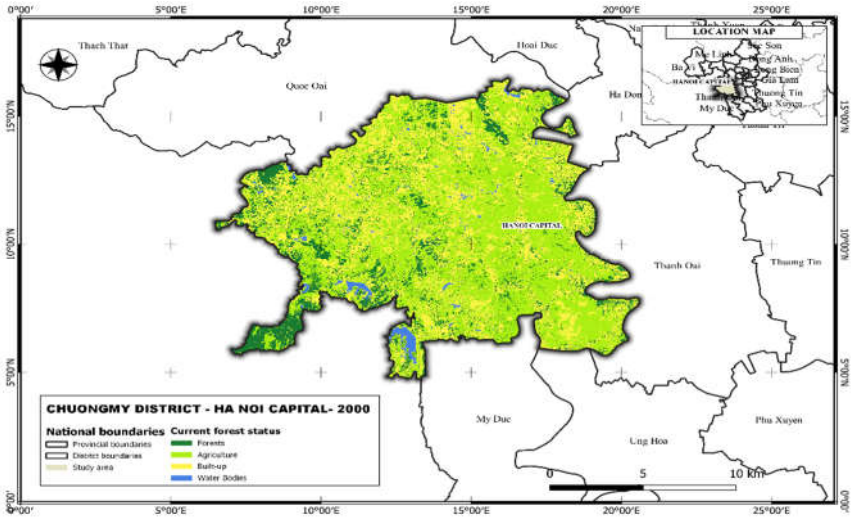

Fig. 1. Geographic location in Chuong My showing land-use and land cover after the conversion took place in Chuong My district

2.2. Methodology

2.2.1. Random Forest algorithm used for land cover classification

Random forest is known as the classification of multi-sourced remote sensing and geography data [15]. The Random Forest (RF) algorithm is considered one of the most accurate land cover classification methods [16]. Therefore, the RF was selected, tested and used for land cover classification in combination with NDVI classifiers in Chuong My district. This method has achieved the best accuracy of land classification and has been confirmed by many studies [17, 18, 19].

The overall accuracy (OA) is known as the total percentage of classification, given by the ratio between the number of correctly classified units and their total number, while User accuracy (UA) and Producer accuracy (PA) are defined as single-class classification accuracies. The UA is the ratio between correctly classified and all classified units in a given class, while the PA is the ratio between the number of correctly classified units and the number of validation units in a given class. In this study, the UA and PA were calculated, for each LC class, as the mean value of all LC classes, UAm (Eq. 1) and PAm (Eq. 2), respectively.

$$UA_m = \frac{\sum_{i=1}^{n} UA}{n} \quad (1)$$

$$PA_m = \frac{\sum_{i=1}^{n} PA}{n} \quad (2)$$

Where n is the number of LC classes.

To assess the accuracy of land cover classification by the Random Forest approach (RF), the study used 100 GPS points collected from the field, allocating to forest class with 30 GPS points, built-up and urban areas (20 GPS points); water (20 GPS points); and agricultural land (30 GPS points).

2.2.2. Land surface temperature (LST) estimation developed in GEE

The algorithm available in GEE was used in this study. GEE has two APIs, namely a JavaScript and a Python interface. Both of them provide libraries of functions of accessing Google's computing and storage infrastructure. This study used the Python API for the land surface temperature derived from the multi-temporal Landsat data (Figs. 3a, 3b, 3c).

Land surface temperature was calculated in the GEE platform and demonstrated in Fig. 2 and Fig. 3a, Fig. 3b, and Fig. 3c.

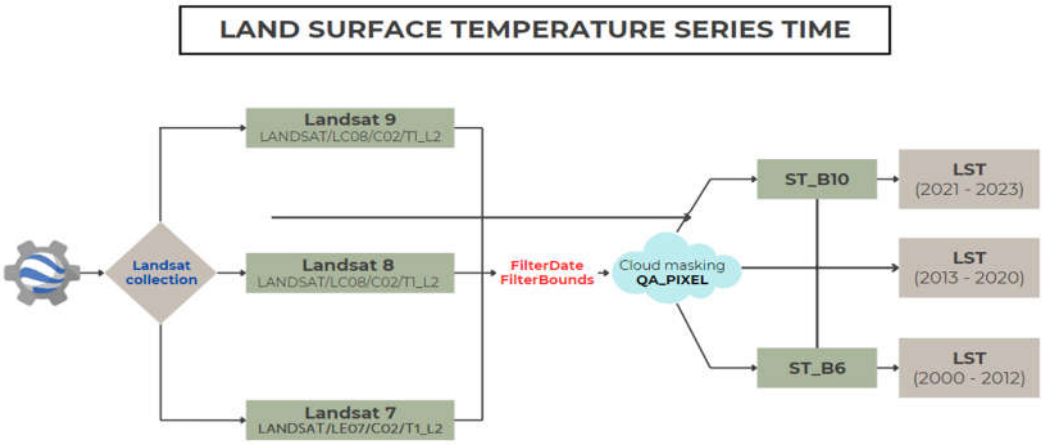

Fig. 2. Flow chart of land surface temperature calculated in GEE platform

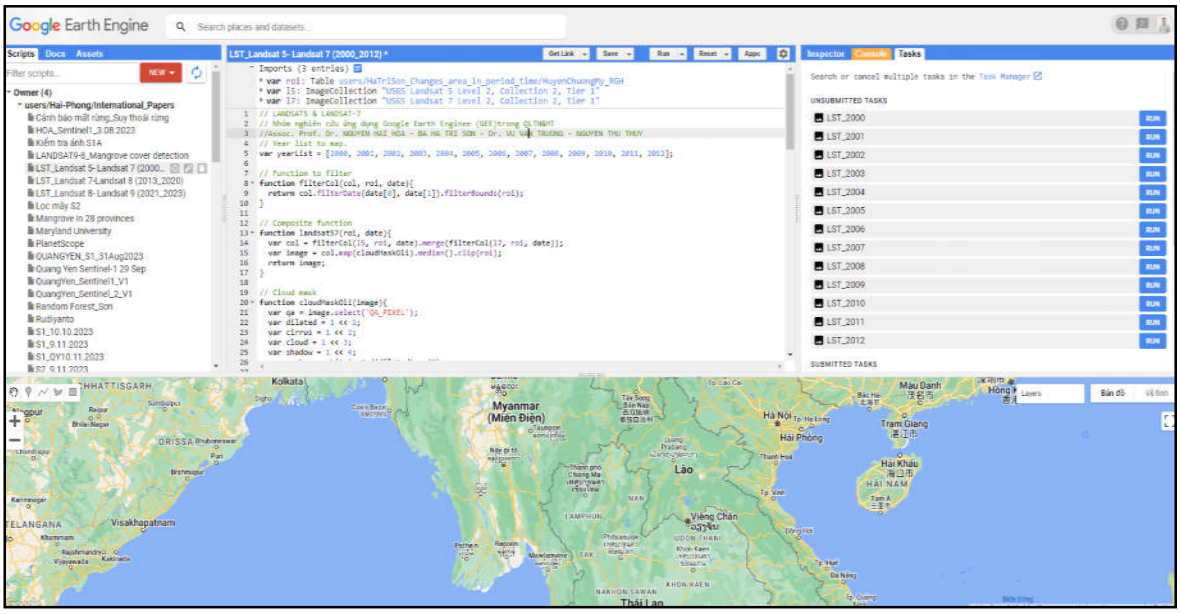

Fig. 3a. Land surface temperature calculated in GEE platform from 2000- 2012 (Landsat-5)

Fig. 3b. Land surface temperature calculated in GEE platform from 2021- 2023 (Landsat-8, Landsat-9)

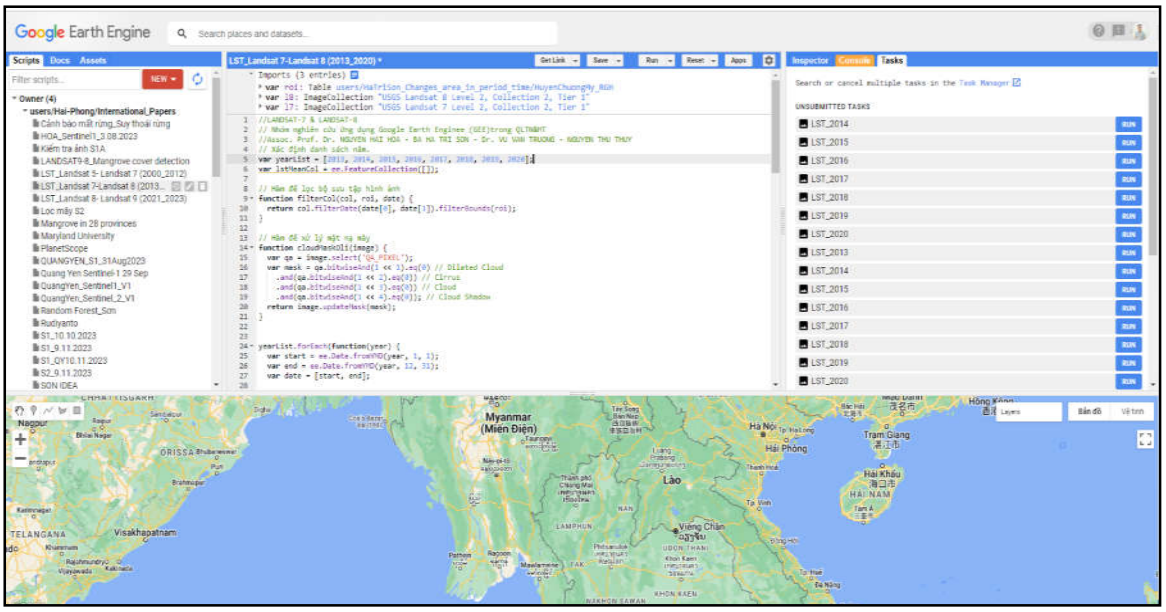

Fig. 3c. Land surface temperature calculated in GEE platform from 2014- 2020 (Landsat-7, Landsat-8)

Table 1. Landsat 5, 7, 8, and 9 thermal bands: wavelengths, spatial resolution and time period covered

Landsat data	Thermal band(s) #	Wavelength (µm)	Spatial resolution (m)
Landsat 5	Band 6	10.40-12.50	120 (30)[a]
Landsat 7	Band 6	10.40-12.50	60 (30)[a]
Landsat 8	Band 10	10.60- 11.19	100 (30)[a]
	Band 11	11.50- 12.51	
Lansdsat 9	Band 10	10.60- 11.19	100 (30)[a]
	Band 11	11.50- 12.51	

Thermal band data are required at a lower resolution and resampled with cubic convolution at a higher spatial resolution before distribution as products by USGS.

2.2.3. Data used for LST estimation

The main source of data in this study includes Landsat 5, 7, 8 and 9 acquisitions, provided by the USGS and included in the GEE data catalogue. GEE provides easy and instant access to satellite products and the computing resources to process them directly on the platform (Fig. 3a, 3b, 3c). Data from various sources and satellites are organised in image collections to allow for their combinations and simultaneous processing. Table 2 indicates the data used for LST estimation along with GEE data catalogue identifier (Table 2).

Table 2. List of products in the GEE catalogue used to estimate the Landsat LST

Data	GEE product identifier
Landsat 5: Radiance at sensor from Band 6	Landsat/LT5_L1T
Landsat 5: Brightness temperature from Band 6	Landsat/LT5_TOA_FMASK
Landsat 7: Radiance at sensor from Band 6	Landsat/LE7_L1T
Landsat 7: Brightness temperature from Band 6	Landsat/LE7_L1T_TOA_FMASK
Landsat 8: Radiance at sensor from Band 10	Landsat/LC8_L1T
Landsat 8: Brightness temperature from Band 10	Landsat/LC8_L1T_TOA_FMASK
Landsat 9: Radiance at sensor from Band 10	Landsat/LC9_L1T
Landsat 9: Brightness temperature from Band 10	Landsat/LC9_L1T_TOA_FMASK
Landsat 5: Surface reflectance product	Landsat/LT5_SR
Landsat 7: Surface reflectance product	Landsat/LE7_L1T_SR
Landsat 8: Surface reflectance product	Landsat/LC8_SR
Landsat 9: Surface reflectance product	Landsat/LC9_SR
Fmask, from extra band in GEE's brightness temperature products	Landsat/LT5_L1T_TOA_FMASK Landsat/LE7_L1T_TOA_FMASK Landsat/LC8_L1T_TOA_FMASK Landsat?LC9_L1T_FMASK

3. RESULTS AND DISCUSSION

Land cover from multi-temporal Landsat data:

To classify the land cover into four classes, including forests, agriculture, urban and built-up areas and water, this study used the thresholds of NDVI, and land cover maps were then constructed among different years (Table 3). As a result, the results showed that NDVI ranged from -0.465 to 0.806, where the higher value of NDVI indicates a denser land cover by vegetation. There are four land cover classes based on the thresholds of NDVI as shown in Table 3.

Table 3. Land cover derived from Landsat data during 2000- 2024 (ha).

Land-cover	2000	2005	2010	2015	2020	2024
Forests	3240.8	2456.6	4515.6	3314.2	3003.3	3601.0
Agriculture	13564.2	14840.8	11539.5	14419.0	12890.1	11373.3
Built-up	6573.3	5328.6	6178.8	5196.2	7043.6	7364.9
Water	467.9	1220.2	1612.2	916.8	909.2	1507.0
Total (ha)	23846.2	23846.2	23846.2	23846.2	23846.2	23846.2

As indicated from Table 3 and Fig. 4, the extent of land cover has changed since 2000. In particular, the tendency of agricultural land has reduced and been replaced by built-up areas, with evidence being an increase of built-up areas from 3573.32 ha (2000) to 4364.92 ha (2024).

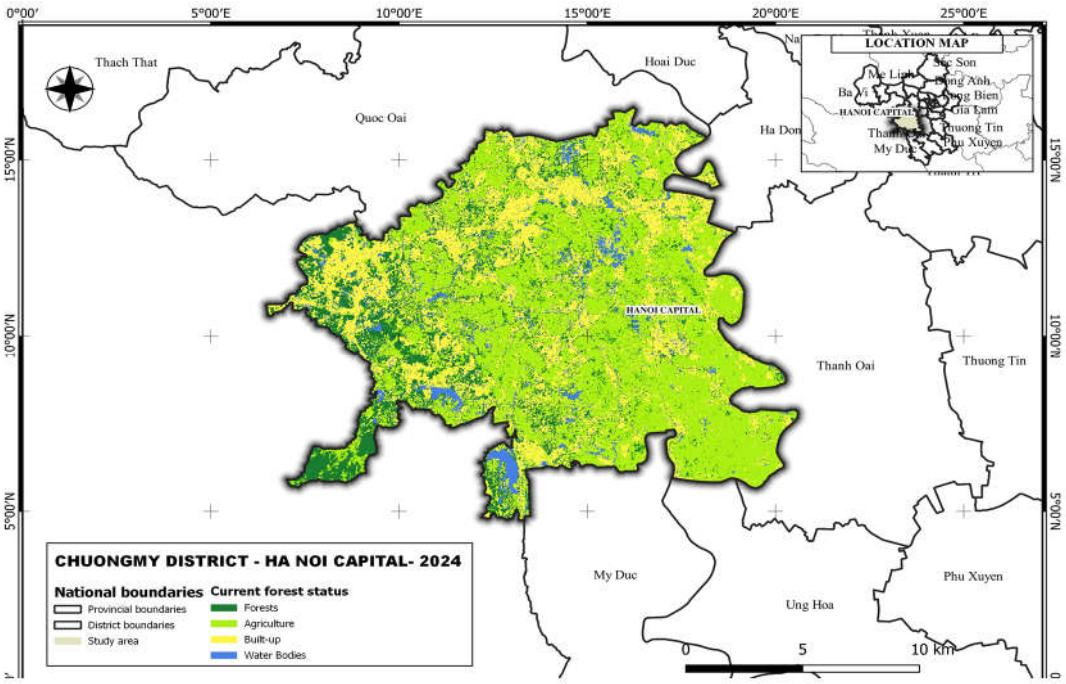

Fig. 4. Land cover derived from Landsat 2024 in Chuong My district

Accuracy assessments of land cover classification:

As a result in 2024 in Table 4, the overall accuracy of land cover classification is 91.9% with Kappa coefficient of 0.89. In particular, forest cover has an accuracy of 81.1%, agricultural land of 96.7%, urban and built-up areas of 92.0%, and water with an accuracy of 94.6%. With the accuracy assessments, the Random Forest classification is reliable and highly accurate in land cover classification from Landsat. In fact, a number of previous studies confirm the reliability of RF classification and its suitability for land cover classification.

Table 4. Accuracy assessments of land cover classification in Chuong My

Land cover	2000		2005		2010		2015		2020		2024	
	UA (%)	PA (%)	UA (%)	PA (%)	UA (%)	PA (%)	UA (%)	PA (%)	UA (%)	PA (%)	UA (%)	PA (%)
Forests	95.0	100.0	97.1	87.2	97.2	94.6	86.8	97.1	100.0	100.0	90.1	81.1
Agriculture	93.0	93.0	79.7	90.8	73.2	81.3	89.1	81. 7	87.7	89.1	88.1	96.7
Built-up	92.0	84.0	87.7	78.1	82.0	75.8	92.1	92.1	91.3	91.3	92.0	92.0
Water	96.0	100.0	95.0	100.0	94.9	92.5	97.6	100.0	100.0	97. 8	100.0	94.6
OA (%)	*94.0*		*87.9*		*84.1*		*91.5*		*93.3*		*91.9*	
Kappa	*0.91*		*0.83*		*0.78*		*0.88*		*0.91*		*0.89*	

**Note: UA (User accuracy); PA (Producer accuracy); OA (Overall accuracy).*

Surface temperature estimation from Landsat:

As a result, land surface temperature derived from Landsat data was summarised in Table 5.

Table 5. Averaged land surface temperature derived from Landsat data in Chuong My district.

Year	Max[1]	Min[1]	Mean[1]	Year	Max[1]	Min[1]	Mean[1]
2000	35.0	20.0	28.8±2.0	2012	37.0	10.0	29.2±4.3
2001	39.0	12.0	33.6±3.0	2013	35.0	19.0	30.4±2.4
2002	37.0	25.0	32.3±2.1	2014	32.0	16.0	28.0±3.1
2003	36.0	15.0	30.0±2.7	2015	42.0	28.0	36.6±2.4
2004	33.0	19.0	29.7±1.6	2016	36.0	22.0	31.6±2.3
2005	40.0	23.0	31.1±2.1	2017	35.0	18.0	30.8±2.4
2006	36.0	21.0	32.4±1.8	2018	38.0	25.0	34.1±2.5
2007	34.0	19.0	29.8±2.2	2019	38.0	19.0	33.0±2.5
2008	34.0	19.0	26.6±2.0	2020	38.0	9.0	33.3±2.8
2009	33.0	13.0	28.3±1.9	2021	43.0	26.0	36.6±3.0
2010	31.0	18.0	27.9±1.9	2022	36.0	23.0	32.8±2.2
2011	37.0	21.0	31.6±2.0	2023	34.0	23.0	35.2±2.6

**Note: [1]Temperature was estimated from Landsat data in the GEE platform.*

Variation of land surface temperature from 2000- 2023:

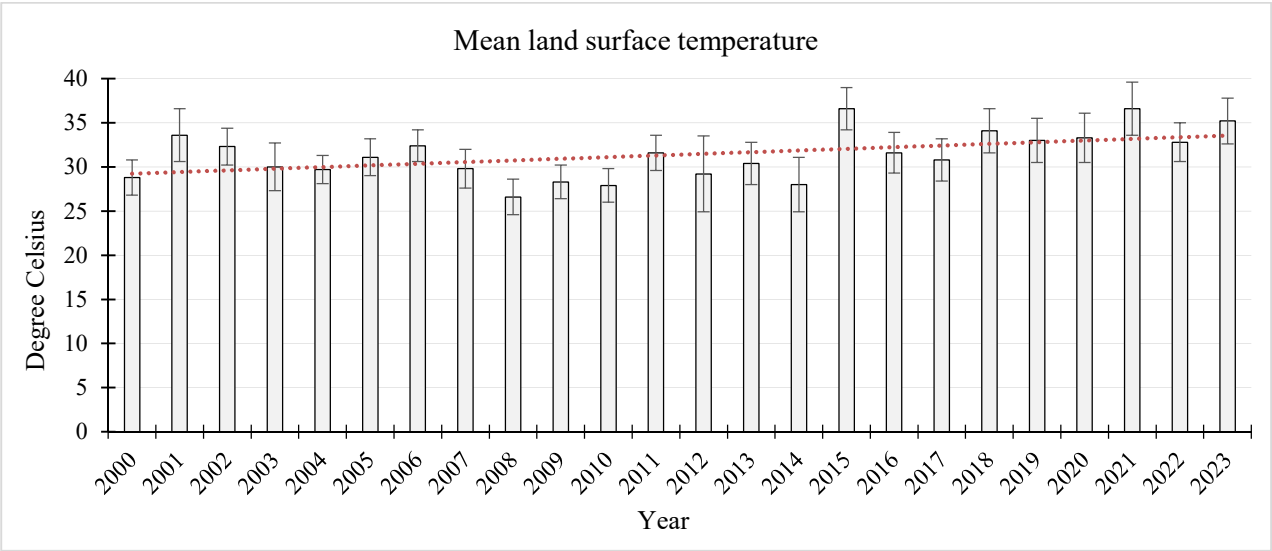

Fig. 5. Variation of land surface temperature derived from Landsat data from 2000-2023

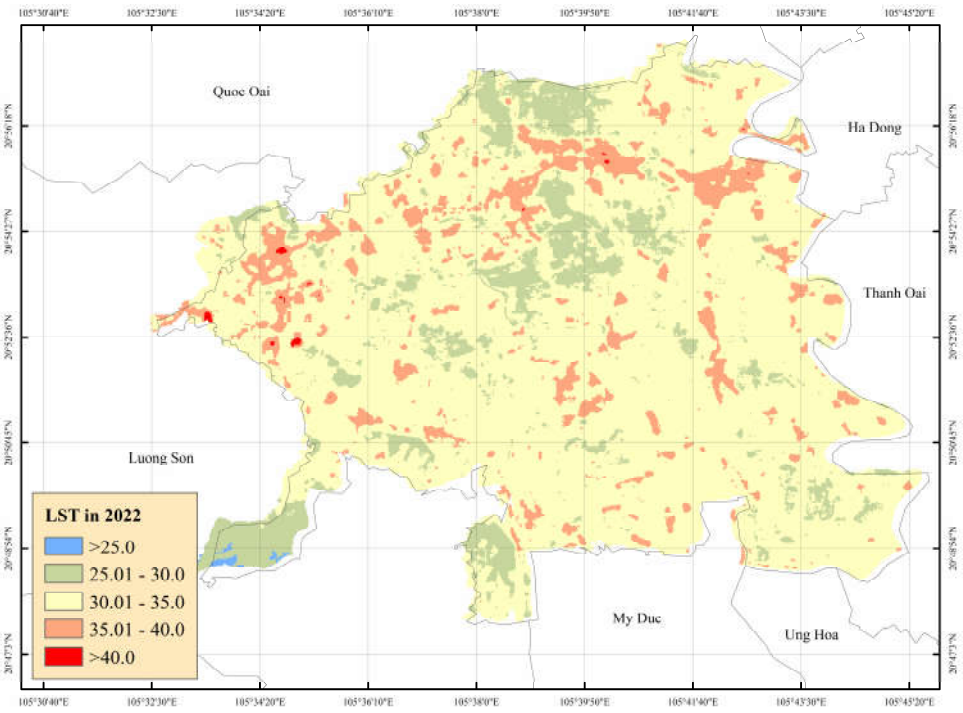

Fig. 6. Land surface temperature in Chuong My from Landsat data in 2022

As shown in Table 5 and Fig. 6, there was a high degree of variability in averaged land surface temperature (LST) from 2000 to 2023, ranging from 26.6^{0}C (2008) to 36.6^{0}C (2023) with the mean of 31.4±2.7^{0}C. However, the data exhibited a greater variation of maximum land surface temperature from 2000-2023, such as the temperatures in 2004 (40^{0}C), 2010 (31^{0}C), 2015 (42^{0}C) and 2021 (43^{0}C), with mean maximum LST of 39.1±2.9^{0}C (Fig. 7). More importantly, these variations imply that there may be a driver of change in LST in Chuong My district.

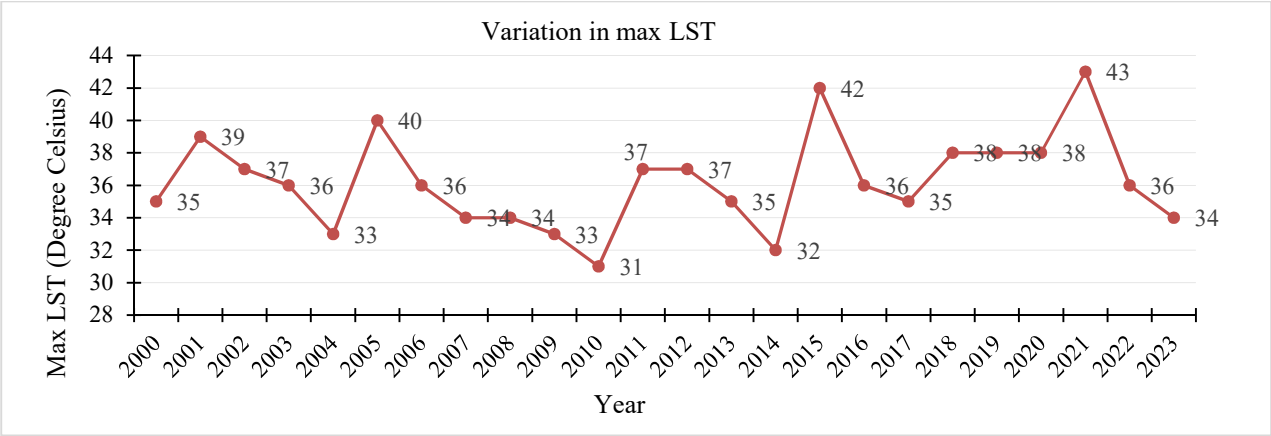

Fig. 7. Variation of max LST derived from Landsat data in Chuong My District

Relationship between surface temperature and land cover:

The analysis of changes in land cover showed a distinct variation over time across the region, especially in industrial and built-up areas between 2000 and 2024. In 2000, there was a pre-period of land-cover conversion driven by industrial, urban areas and built-up expansion, whereas the post-period of the change took place in 2024. The land cover change among periods is summarised in Table 6.

Table 6. Changes in land cover in Chuong My in the period of 2000-2024 (ha)

Land cover	2000	2010	2000-2010	2020	2010-2020	2024	2020-2024	2000-2024
Forest	3240.8	4515.6	1274.8	3003.3	-1512.3	3601.0	5113.3	360.2
Agriculture	13564.2	11539.5	-2024.7	12890.1	1350.6	11.373.3	10022.7	-2190.9
Built-up	6573.3	6178.8	- 394.5	7043.6	864.8	7364.9	6500.1	791.6
Water	467.9	1612.2	1144.4	909.2	-703.1	1507.0	2210.1	1039.1

Table 6 indicates that there has been a change in land cover (extent) for 24 years due to the conversion of land use, partially contributing to an increase of "urban heat island" during the summer. Notably, there was an increase in land surface temperature during the period of 2000- 2023 shown in Figs. 5 and 7. This finding is confirmed by previous studies [20, 21,22]. These studies all confirm that built-up and low vegetated areas are responsible for the high LST and industrial areas frequently appear as urban hot spot. In addition, satellite data, including Landsat data, are suitable for estimating the urban heat island.

4. CONCLUSION

With the application of multi-temporal data in the GEE platform, the study pointed out that the land cover has witnessed significant changes with the main drivers being industrial development and urban and built-up expansion. It is suggested that RF algorithm for the classification and mapping of land cover in 2024 be applied in Chuong My district, whose overall accuracy of land cover mapping is recorded at 91.9% with Kappa coefficient of 0.89. The data for the period from 2000 to 2010 demonstrated the conversion of 327.0 ha of land areas to other land uses such as industrial development, and urban and residential land. There was also a similar continued trend of land conversion into other land use purposes recorded between 2010 and 2024, with a decrease in agricultural land area (65.7 ha) and an increase in industrial land use (65.2 ha). However, it was calculated that the period of 2010-2024 saw a lower rate of conversion than the previous period (2000-2010). The findings found that high LST values were concentrated in urban and industrial areas, with buildings, impermeable pavements and sparse vegetation. Urbanised and poor vegetation areas have high surface urban heat island intensity. The figures for the periods of 2000-2010 and 2010-2024 indicated that the LST has experienced major changes, where most of the LST was recorded with an increase of over 2^0C. Notably, from 2003 to 2025, a total area of 1424 ha underwent an increase of above 3^0C in temperature. The previously mentioned consequences stem from the process of urbanization and industrialization, which first occurred in 2008, as well as the change in land cover status in the study area.

Acknowledgments

This research is funded by Vietnam National University of Forestry. The authors also would like to thank People's Committee and local people in associated communes of Chuong My district, Hanoi city for supporting us when collecting data.

REFERENCES

[1]. Quattrochi D.A. & Luvall J.C. (1999). Thermal infrared remote sensing for analysis of landscape ecological processes: Methods and applications. Landsc. Ecol. 14: 577-598.

[2]. Chrysoulakis N., Lopes M., San José R., Grimmond C.S.B., Jones M.B., Magliulo V., Klostermann, J.E.M., Synnefa, A., Mitraka, Z., Castro E.A., Gonzales A., Vogt R., Vesala T., Spano D., Pigeon G., Freer-Smith P., Staszewski T., Hodges N., Mills G. & Cartalis C. (2013). Sustainable urban metabolism as a link between bio-physical sciences and urban planning: The BRIDGE project. Landsc. Urban Plan. 112: 100-117.

[3]. Anderson M.C., Norman J.M., Kustas W.P.,

Houborg R., Starks P.J. & Agam N. (2008). A thermal-based remote sensing technique for routine mapping of land-surface carbon, water and energy fluxes from field to regional scales. Remote Sens. Environ. 112: 4227-4241.

[4]. Parastatidis D., Mitraka Z., Chrysoulakis N. & Abrams M. (2027). online global Landsat surface temperature estimation from Lansat. Remote Sensing. 9: 1208. https://doi.org/10.3390/rs9121208

[5]. Benas N., Chrysoulakis N. & Cartalis C. (2016). Trends of urban surface temperature and heat island characteristics in the Mediterranean. Theor. Appl. Climatol. 1–10.

[6]. Weng Q., Lu D. & Schubring J. (2004). Estimation of land surface temperature-vegetation abundance relationship for urban heat island studies. Remote Sens. Environ. 89: 467-483.

[7]. Tomlinson C.J., Chapman L., Thornes J.& Baker C. (2011). Remote sensing land surface temperature for meteorology and climatology: A review. Meteorol. Appl. 18: 296-306.

[8]. Jimenez-Munoz J.C., Cristobal J., Sobrino J.A., Sòria G., Ninyerola M. & Pons X. (2009). Revision of the single-channel algorithm for land surface temperature retrieval from Landsat thermal-infrared data. IEEE Trans. Geosci. Remote Sens. 47: 339–349.

[9]. Jimenez-Munoz J.C., Sobrino J.A., Skokovic D., Mattar C. & Cristobal J. (2014). Land surface temperature retrieval methods from Landsat-8 thermal infrared sensor data. IEEE Geosci. Remote Sens. Lett. 11: 1840-1843.

[10]. Quantum Geographic Information System (QGIS). Available online: http://www.qgis.org/en/site/index. html (accessed on 23 May 2024)

[11]. Avdan U. & Jovanovska G. (2016). Algorithm for automated mapping of land surface temperature using Landsat 8 satellite data. J. Sens. 1–8.

[12]. Vo Dai Nguyen, Nguyen Hai Hoa, Nguyen Quyet & Pham Duy Quang. (2021). Land surface temperature responses to vegetation and soil moisture index using Landsat-8 data in Luong Son district, Hoa Binh province. Journal of Forestry Science & Technology. 11: 82-94.

[13]. Nguyen Hai Hoa (2015). Using Landsat data to estimate the changes in land surface temperature and solutions on minimising its impacts in Chuong My ditstrict, Hai Noi during 2000-2015. Journal of Forestry Science & Technology (Translated from Nguyen Hai Hoa).

[14]. Nguyen Khac Manh, Nguyen Hai Hoa, Le Thao Van, Pham Duy Quang & Vo Dai Nguyen (2020). Determing threshold of water indices to detect small surface water areas in wetlands of Chuong My district, Hanoi city. Journal of Forest Science & Technology. 10: 77-87.

[15]. Gislason P.O., Benediktsson J.A. & Sveinsson J.R. (2006). Random Forest for land cover classification. Patter Recognition Letters. 27:294-300. https://doi.org/10.1016/j.patrec.2005.08.011

[16]. Nong Thi Oanh, Tran Xuan Truong, Ta Hoang Trung & Trinh Viet Nga (2023). Automatic model for classification of land cover data for greenhouse gas Inventory using remote sensing imageries. Journal of Geodesy & Cartography. 57(9): 55-64

[17]. Praticò S., Solano F., Di Fazio S. & Modica G. (2021). Machine learning classification of mediterranean forest habitats in Google Earth Engine based on seasonal Sentinel-2 time-series and input image composition optimisation. Remote Sens. 13:586. https://doi.org/10.3390/rs13040586

[18]. Abdel-Rahman E.M., Mutanga O.; Adam E., & Ismail R. (2014). Detecting Sirex octillion grey-attacked and lightning-struck pine trees using airborne hyperspectral data, random forest and support vector machines classifiers. ISPRS J. Photogram. Remote Sens. 88: 48–59. https://doi.org/10.1016/j.isprsjprs.2013.11.013

[19]. Breiman L. (2001). Random Forests. Mach. Learn. 45: 5–32.
https://doi.org/10.1023/A:1010933404324

[20]. Sandoval S., Escobar-Flores J.G. & Munir M.B. (2023). Urbanization and its impacts on land surface temperature and sea surface temperature in a tourist region in Mexico from 1990 to 2020. Remote Sensing Applications: Society and Environment. 101046. https://doi.org/10.1016/j.rsase.2023.101046

[21]. Portela C.I., Massi K.G., Rodrigues T. & Alcantara, E. (2020). Impact of urban and industrial features on land surface temperature: Evidence from satellite thermal indices. Sustainable Cities and Society. 102100. https://doi.org/10.1016/j.scs.2020.102100